

Variability study of classical supergiant X-ray binary 4U 1907+09 using *NuSTAR*

Raj Kumar^{a,b,*}, Sayantan Bhattacharya^c, Sudip Bhattacharyya^c, Subir Bhattacharyya^{a,b}

^a*Astrophysical Sciences Division, Bhabha Atomic Research Centre, Mumbai, 400085, India*

^b*Homi Bhabha National Institute, Mumbai, 400094, India*

^c*Department of Astronomy and Astrophysics, Tata Institute of Fundamental Research, 1 Homi Bhabha Road, Colaba, Mumbai, 400005, India*

Abstract

We investigate the X-ray variability of the supergiant X-ray binary 4U 1907+09 using the new *NuSTAR* observation of 2024. The source had a relatively stable flux level during previous *NuSTAR* observations, but the flux varied significantly during the current one. The light curve exhibits dips (off-state) and flares (on-state). The phase-coherent timing analysis during the on-state yields a pulse period of 443.99(4) s, showing the pulsar's continued spin-down. The pulse profiles show an asymmetric double-peaked structure with a phase separation of 0.47 between the two peaks. A cyclotron resonance scattering feature (CRSF) is also detected at ~ 17.6 keV, along with its harmonic at ~ 38 keV, persisting across all flux states. Flux-resolved spectroscopy reveals that the CRSF remains constant despite a 25-fold change in flux. The spectral parameters like photon index and e-fold energy are out of phase with the pulse shape, whereas cutoff energy is in phase with the pulse shape. The source's luminosity during the on-state is 2.85×10^{35} erg s⁻¹, consistent with a "pencil" beam radiation pattern expected at this flux level from a collisionless gas-mediated shock. These results offer further insights into the accretion dynamics and magnetic field geometry of this system.

Keywords: accretion, X-ray binaries, neutron star X-rays binaries, Accreting pulsar: 4U 1907+09, data analysis

1. Introduction

Supergiant X-ray binaries (sgXBs) are binary systems that consist of a compact object and a massive O/B supergiant star. The accretion of stellar wind from the supergiant star onto a compact object is responsible for the X-ray emission in these systems. There are two types of X-ray binaries: classical supergiant high-mass binaries and supergiant fast X-ray transients (SFXTs) (Pradhan et al., 2018). 4U 1907+09 is a classical supergiant high-mass X-ray binary identified in the third *Uhuru* survey (Giacconi et al., 1971). The pulsar orbiting companion with an eccentricity $e \sim 0.28$ and an orbital period of $P \sim 8.3753$ d (in 't Zand et al., 1998). Optical and infrared studies suggest an O8-O9 Ia type supergiant donor (Cox et al., 2005; Nespoli et al., 2008). The literature reports a source distance of 5 kpc (Cox et al., 2005; Nespoli et al., 2008). However, the distance to the source calculated by Gaia EDR3 is around 1.9 kpc (Bailer-Jones et al., 2021).

X-ray pulsation with a period of 437.5 s was initially reported by Makishima et al. (1984) utilizing *Tenma* observations. Early observations of the source revealed a relatively constant spin-down rate (Baykal et al., 2006); however, further observations revealed several torque reversals and spin-down rate variations (Fritz et al., 2006; Inam et al., 2009). *INTEGRAL* and *RXTE* measurements show short-term fluctuations in the pulse period compared to long-term changes in spin period rates, consistent with the random walk model (Şahiner et al., 2012). The most recent studies reported spin down of the pulsar (Varun et al., 2019; Tobrej et al., 2023).

4U 1907+09 is a variable X-ray source that exhibits irregular flaring and dipping activities. During the dips, in 't Zand et al. (1997) did not detect X-ray pulsed emission from 4U 1907+09 using *RXTE* observations. The typical duration of the dips ranges from a few minutes to 1.5 hours. They suggested that cessation of accretion from the inhomogeneous wind of the companion star may be responsible for dips. Doroshenko et al. (2012) investigated the dipping activity using *Suzaku* observations and found the pulsations during the off state. The transition between off-state (dips) and on-state (nor-

*Corresponding author

Email address: arya95raj@gmail.com (Raj Kumar)

mal flux state) was explained within the framework of “gated accretion”.

The X-ray spectra of 4U 1907+09 are characterized by a power law and an exponential cut-off Schwartz et al. (1980); Marshall and Ricketts (1980); Makishima et al. (1984); Cook and Page (1987); Chitnis et al. (1993); Roberts et al. (2001); Coburn et al. (2002); Baykal et al. (2006); Fritz et al. (2006); Varun et al. (2019); Tobrej et al. (2023). During the binary orbit, inhomogeneous accretion via intense stellar wind caused highly variable hydrogen column density (n_H) ranging from 1×10^{22} to $9 \times 10^{22} \text{ cm}^{-2}$ in 't Zand et al. (1997). Moreover, the spectra showed a narrow spectral line at around 6.4 keV, which is the Fe $K\alpha$ emission caused by the fluorescence of materials near the pulsar. Cyclotron-resonant scattering features (CRSFs) at ~ 19 keV with a second harmonic at ~ 39 keV have been seen using *Ginga* (Mihara, 1995) and *BeppoSAX* observations (Cusumano et al., 1998). This implies a surface magnetic field strength of 2.1×10^{12} G (Cusumano et al., 1998). The flaring activity observed by *AstroSat* indicates that the CRSF parameters have not been altered (Varun et al., 2019). The existence of cyclotron lines at ~ 18 keV and ~ 38 keV were recently verified by Tobrej et al. (2023) utilizing *NuSTAR*. Furthermore, an absorption line possibly due to Ni $K\alpha$ and Ni $K\beta$ at ~ 8 keV was also noticed.

In this work, we have estimated the spin rate and examined the flux-resolved spectral analysis of 4U 1907+09 using *NuSTAR* data observed on 20 November 2024. The manuscript is organized as follows: Section 2 describes observation and data reduction. Section 3 presents the timing and spectral data analysis results. Section 4 discusses the results. Section 5 summarises our findings.

2. Observation and data reduction

NuSTAR is a NASA space mission that observes the sky in the hard X-ray energy band (3-79 keV) of the electromagnetic spectrum (Harrison et al., 2013). It comprises two co-aligned grazing incidence telescopes with specially coated optics and detector units (FPMA and FPMB). In this work, we analyzed the *NuSTAR* data of 4U 1907+09 observed on MJD 60634.

HEASOFT version 6.33 and NuSTARDAS V2.1.2 with CALDBVER 20241126 were used to process and filter the *NuSTAR* event data. We selected a 90 arcsec radius region around the source centroid for the source and a 90 arcsec radius region away from the source for background estimation. The science products: spectra, light curves, and response files were extracted using

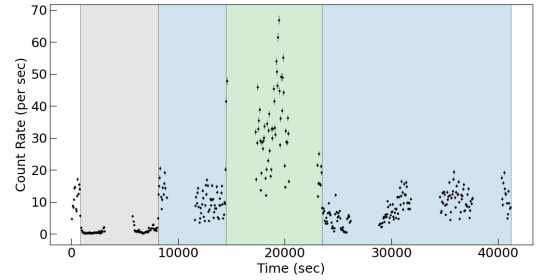


Figure 1: *NuSTAR* light curve of 4U 1907+09 in 3-79 keV energy range for FPMA. The grey-shaded region shows the “off-state”. The blue and green-shaded region shows the “on-state” with low and high flux, respectively. (see section 3)

the `nuproducts` script for both modules (FPMA and FPMB). We extracted the light curves with a time resolution of 0.1 s in the 3-79 keV energy range. The *NuSTAR*/FPMA light curve in the 3-79 keV energy range is shown in Figure 1. The source is largely variable during the observation. We divided the data into off-state and on-state. We extracted spectra and response files for the on and off states. We further divided the on-state into low and high luminosity and extracted the spectra and response files. The `grppha` task was used to rebin the source spectra for a minimum of 30 counts per bin.

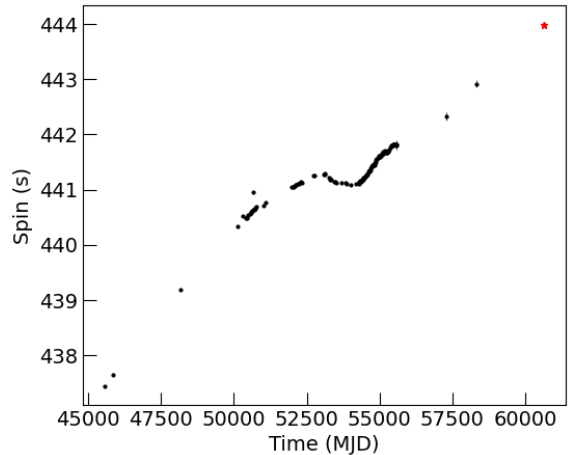


Figure 2: Pulse period history of 4U 1907+09. The pulse period measurements are taken from Cook and Page (1987); in 't Zand et al. (1998); Baykal et al. (2001, 2006); Mukerjee et al. (2001); Fritz et al. (2006); Inam et al. (2009); Şahiner et al. (2012); Varun et al. (2019); Tobrej et al. (2023). The red star corresponds to the spin period estimated in this work. (see section 3.1)

We extracted the light curves during on state with a

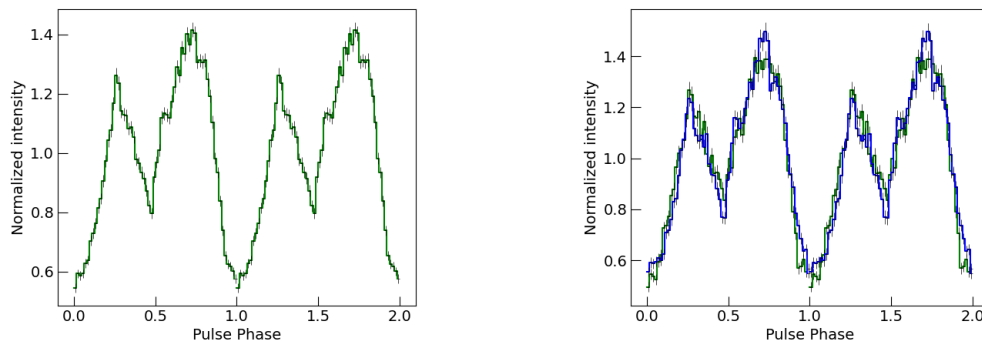


Figure 3: left panel: Pulse profile of 4U 1907+09 in 3-79 keV energy range using FPMA. Right panel: The pulse profile of 4U 1907+09 in high and low flux on-state. The green color corresponds to the low flux state and the blue color corresponds to the high flux state. (sec section 3.1)

time resolution of 0.1 s in the following energy ranges: 3–10 keV, 10–15 keV, 15–20 keV, 20–30 keV, 30–50 keV, and 3–79 keV. We used `barycorr` tool to correct the photon arrival times to the barycenter of the solar system using the DE-430 ephemeris (Folkner et al., 2014).

3. Results

During this *NuSTAR* observation, the source was found to have different X-ray fluxes. We divided the data into off-state and on-state. The effective on-state and off-state exposure are 4.5 ks and 16.5 ks, respectively. Further, we divided the on state into high flux and low flux states. The effective exposure during high flux and low flux in the on state are 4.1 ks and 12.4 ks, respectively. The light curve and different states are shown in Figure 1. First, we performed temporal and spectral analyses on the averaged on-state.

3.1. Timing analysis

We examined the 3-79 keV light curve of averaged on-state for coherent pulsations from the source. We employed the `xronos` tool `efsearch` to estimate the best rotational period. The best period measured in the 3-79 keV energy range is 443.99(4)(MJD 60634.05). The uncertainty in the period was estimated using the bootstrap method by simulating 1000 light curves (Boldin et al., 2013). The calculated pulse period value with pulse period history of 4U 1907+09 is shown in Figure 2. The source was found to be in a spin-down phase. We employed the `efold` technique (Leahy et al., 1983) to create folded light curves at the best period in 3-79 keV, 3-10 keV, 10-15 keV, 15-20 keV, 20-30 keV and 30-50 keV. The left panel of Figure 3 shows the

pulse profile in the 3-79 keV energy range. Figure 4 depicts the pulse shape in different energy ranges. There is a noticeable energy dependence in the pulse profile. A double-peaked feature is visible in the 3-79 keV energy range. This feature dominates in the 3-10 and 10-15 keV energy range. The peak at ~ 0.25 starts to fade after the 15 keV. The pulse fraction (PF) is calculated using the expression,

$$PF = \frac{(I_{\max} - I_{\min})}{(I_{\max} + I_{\min})}$$

Where I_{\max} is the maximum normalized luminosity and I_{\min} is the minimum normalized luminosity. The energy-dependent PF is shown in Figure 5. We checked the flux-dependent pulse shape as shown in the right panel of Figure 3. The pulse shape is similar in both low and high flux on-states.

3.2. Spectral analysis

3.2.1. Averaged on state spectral analysis

We used XSPEC V12.14.0h (Arnaud, 1996) for spectral modeling of the data. A power-law model along with an energy cutoff and smoothing function, is used to represent the continuum spectra observed in X-ray pulsars. We fitted the data by model: `const*tbabs(highecut*pow)`. The model `const` cross-calibrates instruments FPMA and FPMB. `tbabs` is Tuebingen-Boulder interstellar medium absorption model. `pow` is the photon power-law model. `highecut` is the high energy cutoff model given by,

$$M(E) = \begin{cases} \exp\left[-(E_c - E)/E_f\right] & E \geq E_c \\ 1.0 & E \leq E_c \end{cases}$$

where E_c is cutoff energy (keV) and E_f is e-folding energy (keV). The data does not effectively constrain

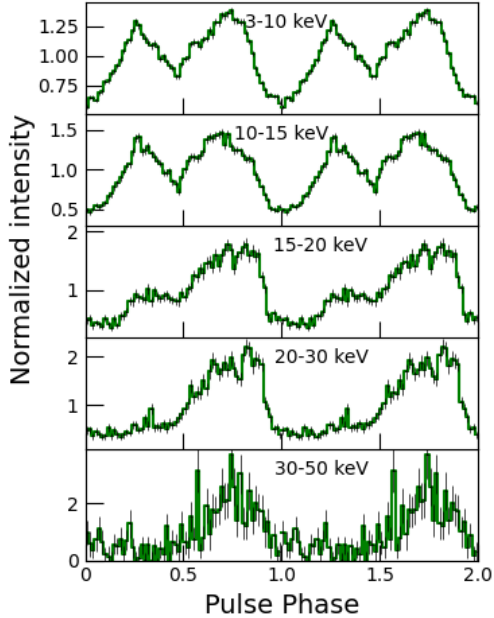


Figure 4: Energy-dependent pulse profiles of 4U 1907+09 using FPMA. The energy range for the pulse profiles is specified inside the panels. (see section 3.1)

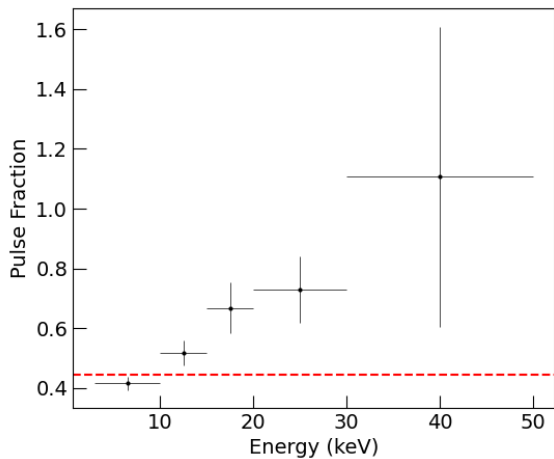


Figure 5: The energy dependence of pulse fraction. The dashed red line corresponds to the pulse fraction in the 3-79 keV energy range. (see section 3.1)

the column density. So, we fixed the n_H value at $1.5 \times 10^{22} \text{ cm}^{-2}$ (Maitra and Paul, 2013; Varun et al., 2019). The χ^2/dof comes out to be $\sim 2202/1119$. An iron line and absorption features around 18 keV and 35 keV due to cyclotron absorption are visible in the residual. So, we added model gauss for the Fe feature and a multiplicative model gabs. So, we added model gauss for the Fe feature and a multiplicative model gabs. The model becomes $\text{const*tbabs}(\text{gauss}+\text{highcut*pow})*\text{gabs}*gabs$. The χ^2/dof improved to $\sim 1277/1110$. The best fitting gives the $\Gamma \sim 1.12$ and $E_{\text{cutoff}} \sim 11.8 \text{ keV}$ and $E_{\text{fold}} \sim 12.8 \text{ keV}$. The Gaussian line is fitted at 6.31 keV with an equivalent width equal to 46 eV, and the absorption lines came out at 17.6 keV and 38.02 keV. The flux came out to be $6.59^{+0.04}_{-0.04} \times 10^{-10} \text{ erg/cm}^2/\text{s}$. To assess the importance of the absorption features in the spectra, we used the `simftest` script from `xspec`. It uses Monte Carlo simulations to produce simulated data sets from the original data, which are then used to estimate $\Delta\chi^2$ for gabs components. We conducted 10^4 simulations for each gabs component. The $\Delta\chi^2$ obtained from simulated data sets is considerably low compared to the observed value for each gabs component. It confirms the significant detection of absorption features at $\sim 17.6 \text{ keV}$ and $\sim 38.02 \text{ keV}$.

Then we fitted the data by model $\text{const*tbabs}(\text{gauss}+\text{compTT})*\text{gabs}*gabs$. `compTT` (Titarchuk, 1994) is an analytic model describing the Comptonization of soft photons in hot plasma and is suitable for describing the continuum shape from X-ray Pulsars. The seed soft photon temperature, plasma temperature, and plasma optical depth are $\sim 0.52 \text{ keV}$, $\sim 7.87 \text{ keV}$, and ~ 6.26 , respectively. The χ^2/dof for this model is $\sim 1285/1110$ which is slightly higher than the previous model.

Finally, we employed the `compmag` (Farinelli et al., 2012) model to fit the continuum spectra. The `compmag` model describes the spectral formation in the accretion column onto the polar cap of a magnetized neutron star, taking into account both thermal and bulk Comptonization processes. Since the magnetic field of 4U 1907+09 is $2 \times 10^{12} \text{ G}$, the `compmag` model is suitable for this system. The model becomes $\text{const*tbabs}(\text{gauss}+\text{bbodyrad}+\text{compmag})*\text{gabs}*gabs$. During the fitting, we consider that the accretion velocity increases towards the NS (by fixing `betaflag=1`) with the index of velocity profile $\eta = 0.5$ and terminal velocity at the NS surface $\beta_0 = 0.05$. We fixed the accretion column $r_0 = 0.25$ (in units of the NS

Schwarzschild radius) and NS albedo $A = 1$. Since the norm of `compmag` is given by R_{km}^2/D_{10}^2 , where R_{km} is the radius of the accretion column in km and D_{10} is the distance of the source in units of 10 kpc. Considering the radius of the accretion column is 1 km and the source distance is equal to 1.9 kpc. We fixed the norm at 28. The temperature of seed blackbody temperature (kT_{bb}) of `compmag` is tied with the blackbody temperature of `bbodyrad`. The remaining parameters of this spectral model were kept free. The χ^2/dof for this model is 1236/1110. The optical depth of the accretion column comes out to be ~ 1.75 . Since the `compmag` model is applicable for $\tau > 1$, we did not further use this model. Also, the low luminosity of the source disfavors the formation of the accretion column. The spectral parameters for different models used in this work are given in Table 1. The *NuSTAR* spectra with residuals of different models used in this work are shown in Figure 6.

3.2.2. Phase resolved Spectroscopy

We extracted the spectral files into eight phases: 0-0.125, 0.125-0.25, 0.25-0.375, 0.375-0.5, 0.5-0.625, 0.625-0.75, 0.75-875, and 0.875-1.0. We fitted the spectral data with the model: `const*tbabs*(highcut*pow)gabs`. The variation of different spectral parameters with phase is given in Figure 7. The top panel provides the 3.0-25.0 keV flux at various pulse phases, facilitating comparison with the pulse profile. The continuum fit parameters exhibit substantial fluctuation with the pulse phase. The cutoff energy and CRSF line center are correlated (in phase) with the pulse shape, whereas the e-fold energy and the photon index are out of phase with the pulse profile.

3.2.3. Flux resolved spectral analysis

As shown in Figure 1, 4U 1907+09 shows the flux variation in the light curve. The spectral data for the off-state, low-flux on-state, and high-flux on-state is shown in Figure 8. We fitted the off-state and high-flux on-state data with the model `const*tbabs(bbodyrad+highcut*pow)*gabs`. The low flux on-state data required additional models `gabs` and `gauss`. We fitted the low flux on-state data with the model. `const*tbabs(gauss+bbodyrad+highcut*pow)*gabs*gabs`. The Γ for off-state, high flux on-state, and low flux on-state come out to be ~ 1.43 , ~ 1.12 , and ~ 1.08 , respectively. At various flux levels, the cyclotron line is found at ~ 18 keV. The line width of CRSF during high flux on-state and low flux on-state are ~ 3.07 and ~ 2.5 , respectively. Compared to low

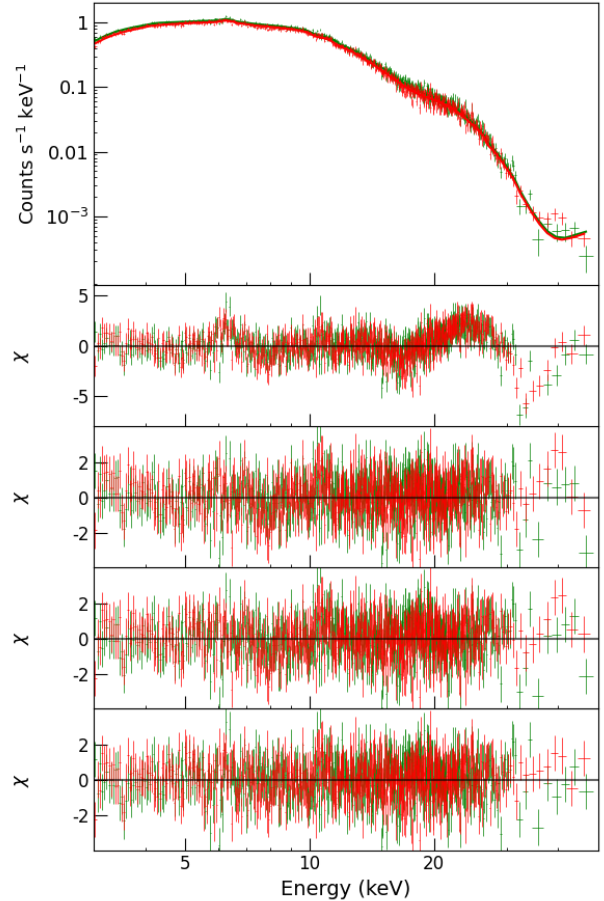


Figure 6: Top: The *NuSTAR* spectra of 4U 1907+09. The green and red colour corresponds to FPMA and FPMB data, respectively. Second panel: residual of the continuum only model-`const*tbabs(highcut*pow)`. The emission line at 6.5 keV and absorption features at 18 keV and 35 keV are visible. Third panel: residual of the model-`const*tbabs(gauss+highcut*pow)gabs*gabs`. Fourth panel: residual of the model-`const*tbabs(gauss++compTT)gabs*gabs`. Bottom panel: residual of the model-`const*tbabs(gauss+bbodyrad+compmag)gabs*gabs`. (see section 3.2)

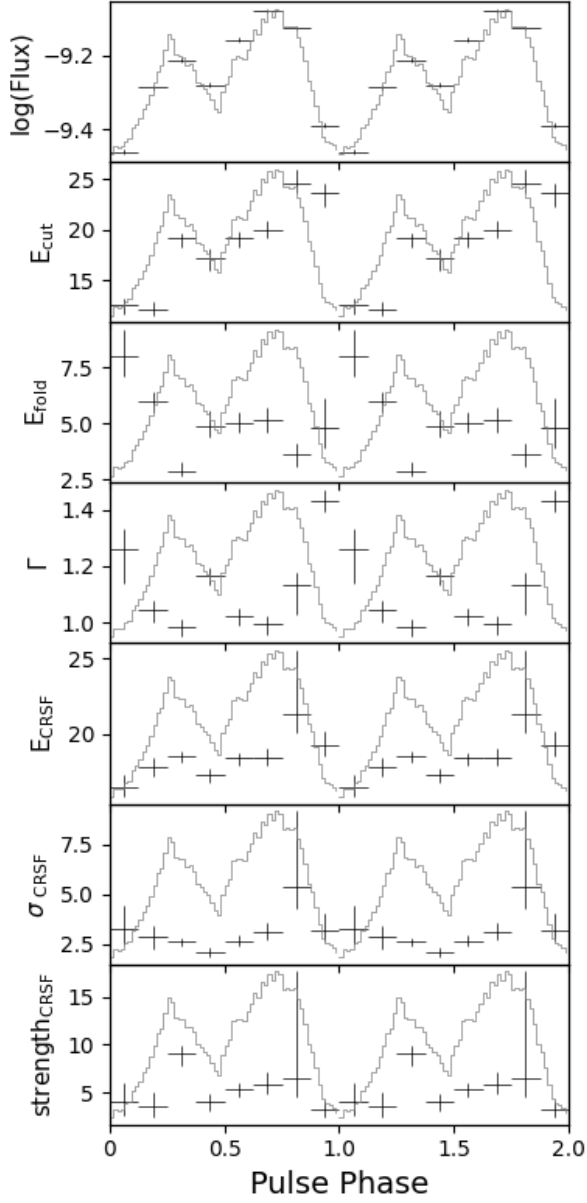


Figure 7: Phase resolved spectroscopy of 4U 1907+09. The flux is calculated in the 3-25 keV energy range. (see section 3.2.2)

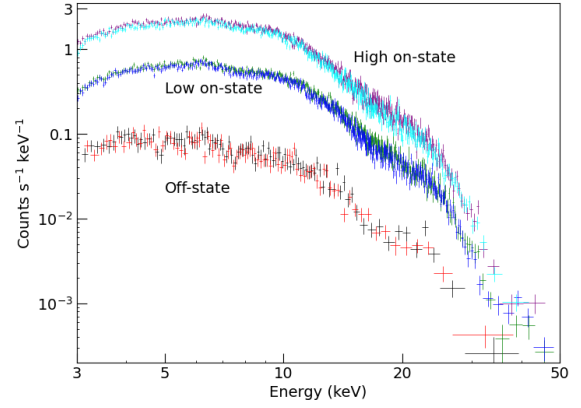


Figure 8: The spectral data of 4U 1907+09 in off-state, low and high flux on-state. (see section 3.2.3)

flux on state, flux increased 3 times during high flux on state, and flux decreased 8 times during off-state. The e-folding energy during the high flux on-state and low flux on-state are ~ 4.6 and ~ 6.27 , respectively. The spectral parameters for each data are given in Table 2.

4. Discussion

4U 1907+09 is a classical supergiant X-ray binary known to show the dips and flares in its light curve. In this work, we analyzed the *NuSTAR* data of 4U 1907+09 observed during November 2024. The spin down/spin up and torque reversals of the pulsar were documented in several studies (Cook and Page, 1987; in 't Zand et al., 1998; Baykal et al., 2001, 2006; Mukerjee et al., 2001; Fritz et al., 2006; Inam et al., 2009; Şahiner et al., 2012; Varun et al., 2019; Tobrej et al., 2023). In the most recent study, Tobrej et al. (2023) found that the 4U 1907+09 has been spinning down. In this work, we estimated the pulse period of 4U 1907+09 to be $\sim 443.99(4)$ s. This indicates that the source is still spinning down. The pulse profile is one of the indicators of the emission region from the neutron star. A double-peaked (at ~ 0.26 and 0.73) asymmetric pulse shape was observed in 4U 1907+09, as shown in the left panel of Figure 3. A similar pulse shape was also reported for the 4U 1907+09 in the previous studies (Maitra and Paul, 2013; Varun et al., 2019; Tobrej et al., 2023). The observed asymmetric pulse shape is most likely caused by a magnetic dipole offset from the rotational axis of the pulsar (Parmar et al., 1989; Leahy, 1991; Riffert et al., 1993; Bulik et al., 1995). Another plausible explanation for the asymmetric shape of pulse

Table 1: Best-fitting spectral parameters of 4U 1907+09 for different spectral models. The hydrogen column density (N_H) is fixed at $1.5 \times 10^{22} \text{ cm}^{-2}$. Errors are reported at 90% confidence level.

Components	Parameters	M1	M2	M3
Const	C_{FPMB}	$1.003^{+0.006}_{-0.006}$	$1.004^{+0.006}_{-0.006}$	$1.004^{+0.005}_{-0.005}$
Powerlaw	Γ	$1.12^{+0.10}_{-0.10}$	-	-
	Norm	$3.12^{+0.06}_{-0.06} \times 10^{-2}$	-	-
highcut	$E_{\text{cutoff}}(\text{keV})$	$11.8^{+0.3}_{-0.3}$	-	-
	$E_{\text{fold}}(\text{keV})$	$12.8^{+1.8}_{-1.0}$	-	-
compTT	$T0(\text{keV})$	-	$0.52^{+0.07}_{-0.15}$	-
	$kT_e(\text{keV})$	-	$7.87^{+2.50}_{-1.38}$	-
	τ	-	$6.26^{+0.27}_{-0.17}$	-
	norm ($\times 10^{-2}$)	-	$1.39^{+0.21}_{-0.08}$	-
compmag	$kT_e(\text{keV})$	-	-	$3.40^{+0.15}_{-0.10}$
	τ	-	-	$1.75^{+0.19}_{-0.14}$
bbbodyrad	$kT_{\text{bb}}(\text{keV})$	-	-	$0.90^{+0.03}_{-0.04}$
	norm	-	-	$18.5^{+5.0}_{-2.6}$
gabs1	$E_{\text{CRSF}}(\text{keV})$	$17.60^{+0.12}_{-0.24}$	$17.95^{+0.16}_{-0.14}$	$17.60^{+0.30}_{-0.24}$
	$\sigma_{\text{CRSF}}(\text{keV})$	$2.23^{+0.47}_{-0.36}$	$2.88^{+0.15}_{-0.13}$	$2.68^{+0.42}_{-0.27}$
	strength	$1.78^{+0.47}_{-0.36}$	$4.47^{+0.51}_{-0.36}$	$3.06^{+1.19}_{-0.52}$
gabs2	$E_{\text{CRSF}}(\text{keV})$	$38.02^{+0.89}_{-0.82}$	$39.55^{+0.72}_{-1.29}$	$34.93^{+0.94}_{-0.66}$
	$\sigma_{\text{CRSF}}(\text{keV})$	$5.88^{+0.98}_{-0.80}$	$10.00^{+1.33}_{-1.10}$	$4.04^{+1.67}_{-0.82}$
	strength	$28.44^{+8.88}_{-5.97}$	$84.41^{+8.89}_{-25.15}$	$11.20^{+7.12}_{-2.94}$
gauss	$E_{\text{Fe}}(\text{keV})$	$6.31^{+0.05}_{-0.06}$	$6.29^{+0.06}_{-0.07}$	$6.18^{+0.11}_{-0.07}$
	$\sigma_{\text{Fe}}(\text{keV})$	$0.11^{+0.12}_{-0.11}$	$0.24^{+0.13}_{-0.11}$	$0.64^{+0.16}_{-0.15}$
	norm ($\times 10^{-4}$)	$1.82^{+0.52}_{-0.45}$	$2.78^{+0.73}_{-0.62}$	$7.91^{+0.25}_{-0.22}$
	EQW (eV)	46	70	207
χ^2/dof		1277/1110	1285/1110	1236/1110

M1: const*tbabs(gauss+highcut*powerlaw)*gabs*gabs

M2: const*tbabs(gauss+compTT)*gabs*gabs

M3: const*tbabs(gauss+bbbodyrad+compmag)*gabs*gabs

Table 2: Best-fitting spectral parameters for off-state, low flux on-state and high flux on-state. The hydrogen column density (N_H) is fixed at $1.5 \times 10^{22} \text{ cm}^{-2}$. The unit of flux is $(\times 10^{-10}) \text{ erg cm}^{-2} \text{ s}^{-1}$. Errors are reported at 90% confidence level.

Components	Parameters	off-state	High flux on-state	Low-flux on-state
Const	C_{FPMB}	$0.977^{+0.043}_{-0.041}$	$0.996^{+0.008}_{-0.008}$	$1.009^{+0.009}_{-0.009}$
Powerlaw	Γ	$1.43^{+0.07}_{-0.07}$	$1.12^{+0.02}_{-0.02}$	$1.08^{+0.02}_{-0.02}$
	Norm	$4.34^{+0.61}_{-0.53} \times 10^{-3}$	$6.59^{+0.21}_{-0.20} \times 10^{-2}$	$1.84^{+0.06}_{-0.05} \times 10^{-2}$
highcut	$E_{\text{cutoff}}(\text{keV})$	$22.9^{+1.1}_{-2.5}$	$19.3^{+0.51}_{-0.78}$	$18.26^{+0.41}_{-0.50}$
	$E_{\text{fold}}(\text{keV})$	$4.6^{+2.8}_{-1.5}$	$4.6^{+0.37}_{-0.25}$	$6.27^{+0.56}_{-0.42}$
gabs1	$E_{\text{CRSF}}(\text{keV})$	$18.56^{+0.64}_{-0.61}$	$18.31^{+0.31}_{-0.43}$	$18.09^{+0.24}_{-0.23}$
	$\sigma_{\text{CRSF}}(\text{keV})$	$2.20^{+0.53}_{-0.44}$	$3.07^{+0.19}_{-0.24}$	$2.50^{+0.15}_{-0.13}$
	strength	$3.43^{+1.10}_{-0.99}$	$6.64^{+0.67}_{-0.84}$	$5.05^{+0.45}_{-0.43}$
gabs2	$E_{\text{CRSF}}(\text{keV})$	-	-	$33.69^{+0.95}_{-0.83}$
	$\sigma_{\text{CRSF}}(\text{keV})$	-	-	$2.99^{+1.28}_{-0.76}$
	strength	-	-	$5.68^{+3.62}_{-2.00}$
gauss	$E_{\text{Fe}}(\text{keV})$	-	-	$6.26^{+0.07}_{-0.08}$
	$\sigma_{\text{Fe}}(\text{keV})$	-	-	$0.16^{+0.11}_{-0.13}$
	norm ($\times 10^{-4}$)	-	-	$1.54^{+0.46}_{-0.41}$
flux _{3-25 keV}		$0.472^{+0.016}_{-0.016}$	$12.156^{+0.080}_{-0.078}$	$3.910^{+0.026}_{-0.026}$
χ^2/dof		205/181	1045/929	1047/940

profiles is an asymmetric accretion stream (Basko and Sunyaev, 1976; Wang and Welter, 1981; Miller, 1996). As energy increases, the pulse shape changes significantly. The peak at 0.26 begins to fade at 15 keV. The PF followed an increasing behaviour with energy.

The *NuSTAR* spectrum was fitted with three different models: power law with `highcut`, `compTT`, and `compmag`. Table 1 contains the corresponding fit parameters. The iron line and CRSF with its harmonic were found at ~ 6.31 keV, ~ 17.6 keV, and ~ 38.02 keV, respectively. After incorporating gravitational redshift, the CRSF corresponds to a magnetic field of $\sim 2 \times 10^{12}$ G. The average flux of the source during the on-state in the 3–50 keV energy range was found to be $\sim 6.59 \times 10^{-10}$ erg cm $^{-2}$ s $^{-1}$. Assuming a distance of 1.9 kpc, the estimated luminosity of the source is $\sim 2.85 \times 10^{35}$ erg s $^{-1}$. The luminosity of the source is similar to that observed by *NuSTAR* in 2018 (Tobrej et al., 2023). Using the formalism in Becker et al. (2012), we estimate the critical luminosity $L_{\text{crit}} = 1.5 \times 10^{37} \left(\frac{B}{10^{12} \text{ G}}\right)^{16/15}$ erg s $^{-1}$ to be 3×10^{37} erg s $^{-1}$. The Coulomb braking luminosity $L_{\text{coul}} = 1.2 \times 10^{37} \left(\frac{B}{10^{12} \text{ G}}\right)^{1/3}$ erg s $^{-1}$ to be 1.5×10^{37} erg s $^{-1}$ (Becker et al., 2012; Langer and Rappaport, 1982). The observed luminosity of 4U 1907+09 is much lower than the L_{crit} and L_{coul} . As a result, radiation from a gas-mediated shock without collision is anticipated. This leads to a "pencil" beam, where the radiation is emitted mostly along the magnetic field lines.

Numerous studies examine the dips and flares in the light curve of 4U 1907+09 (in 't Zand et al., 1997; Doroshenko et al., 2012; Şahiner et al., 2012; Shakura et al., 2012; Varun et al., 2019). Apart from 4U 1907+09, off-states or dips have been reported in the Vela X-1 (Kreykenbohm et al., 2008; Doroshenko et al., 2011) and GX 301-2 (Göğüş et al., 2011). Previous studies have ruled out the likelihood of dips generated by a dense, clumpy wind obscuring the neutron star (Fürst et al., 2011; Şahiner et al., 2012). Shakura et al. (2012) suggested that the onset of the off-state in these systems is due to the transition from the Compton cooling-dominated to the radiative cooling-dominated regime. During this observation, the source showed the dip and flare in the light curve. During the dip, the flux of the source decreased 8 times the flux during the low flux on-state. The flux during high flux on-state increased 3 times during low flux on-state. As the flux varied during the on-state, the pulse profile did not differ much and followed a similar trend (as shown in the right panel of Figure 3). It indicates that the emission process did not change during the flare activity. The spectral

modelling of 4U 1907+09 revealed that the E_{CRSF} is unaltered at ~ 18 keV in both the high flux (flare) on-state and the off-state. It suggests that the accretion column may not be formed. The e-folding energy during the high flux on-state is lower than the low flux high state. It shows that the high flux on-state is softer than the low flux on-state. The line width of the CRSF during the high flux on-state is higher than the low flux on-state.

5. Summary

The results and findings of this work are summarized as follows:

- 4U 1907+09 exhibiting normal flux, flare, and dip (off-state) in the light curve and providing insights into the variability of the source.
- With an estimated pulse period of 443.99(4) s, the source was determined to be spin down.
- During the on-state, the typical spectral and temporal characteristics of 4U 1907+09 are detected, including a double-peaked pulse profile, energy dependence of pulse profile, CRSF, and dips in the light curve.
- The CRSF at ~ 18 keV was found in both on and off states. The width of CRSF correlated positively with the flux.
- The spin phase influenced the spectral properties. Cutoff energy is in phase with the pulse shape, but photon index and e-fold energy are out of phase.

Acknowledgments

We have utilized the archived *NuSTAR* data provided by the High Energy Astrophysics Science Archive Research Center (HEASARC) online service maintained by the Goddard Space Flight Center. For this work, we have made use of the *NuSTAR* Data Analysis Software (NuSTARDAS) jointly developed by the ASI Space Science Data Center (SSDC, Italy) and the California Institute of Technology (Caltech, USA). RK acknowledges the Department of Astronomy and Astrophysics, Tata Institute of Fundamental Research, Mumbai, India for providing research facilities.

References

- Arnaud, K.A., 1996. XSPEC: The First Ten Years, in: Jacoby, G.H., Barnes, J. (Eds.), *Astronomical Data Analysis Software and Systems V*, p. 17.

- Bailer-Jones, C.A.L., Rybizki, J., Fouesneau, M., Demleitner, M., Andrae, R., 2021. Estimating Distances from Parallaxes. V. Geometric and Photogeometric Distances to 1.47 Billion Stars in Gaia Early Data Release 3. *aj* 161, 147. doi:10.3847/1538-3881/abd806, arXiv:2012.05220.
- Basko, M.M., Sunyaev, R.A., 1976. The limiting luminosity of accreting neutron stars with magnetic fields. *mnras* 175, 395–417. doi:10.1093/mnr/175.2.395.
- Baykal, A., Inam, Ç., Ali Alpar, M., in't Zand, J., Strohmayer, T., 2001. The steady spin-down rate of 4U 1907+09. *mnras* 327, 1269–1272. doi:10.1046/j.1365-8711.2001.04804.x, arXiv:astro-ph/0011404.
- Baykal, A., Inam, S.Ç., Beklen, E., 2006. Evidence of a change in the long-term spin-down rate of the X-ray pulsar 4U 1907+09. *mnras* 369, 1760–1764. doi:10.1111/j.1365-2966.2006.10412.x, arXiv:astro-ph/0512176.
- Becker, P.A., Klochkov, D., Schönherr, G., Nishimura, O., Ferrigno, C., Caballero, I., Kretschmar, P., Wolff, M.T., Wilms, J., Staubert, R., 2012. Spectral formation in accreting X-ray pulsars: bimodal variation of the cyclotron energy with luminosity. *aap* 544, A123. doi:10.1051/0004-6361/201219065, arXiv:1205.5316.
- Boldin, P.A., Tsygankov, S.S., Lutovinov, A.A., 2013. On timing and spectral characteristics of the X-ray pulsar 4U 0115+63: Evolution of the pulsation period and the cyclotron line energy. *Astronomy Letters* 39, 375–388. doi:10.1134/S1063773713060029, arXiv:1305.6785.
- Bulik, T., Riffert, H., Meszaros, P., Makishima, K., Mihara, T., Thomas, B., 1995. Geometry and Pulse Profiles of X-Ray Pulsars: Asymmetric Relativistic FITS to 4U 1538-52 and VELA X-1. *apj* 444, 405. doi:10.1086/175614.
- Chitnis, V.R., Rao, A.R., Agrawal, P.C., Manchanda, R.K., 1993. Hard X-ray spectrum of 4U 1907+09. *aap* 268, 609–614.
- Coburn, W., Heindl, W.A., Rothschild, R.E., Gruber, D.E., Kreykenbohm, I., Wilms, J., Kretschmar, P., Staubert, R., 2002. Magnetic Fields of Accreting X-Ray Pulsars with the Rossi X-Ray Timing Explorer. *apj* 580, 394–412. doi:10.1086/343033, arXiv:astro-ph/0207325.
- Cook, M.C., Page, C.G., 1987. The X-ray properties of 3A 1907+09. *mnras* 225, 381–392. doi:10.1093/mnr/225.2.381.
- Cox, N.L.J., Kaper, L., Mokiem, M.R., 2005. VLT/UVES spectroscopy of the O supergiant companion to $\dot{\iota}$ ASTROBJ₄U 1907+09/ $\dot{\iota}$ ASTROBJ₄(7). *aap* 436, 661–669. doi:10.1051/0004-6361:20040511.
- Şahiner, Ş., Inam, S.Ç., Baykal, A., 2012. A comprehensive study of RXTE and INTEGRAL observations of the X-ray pulsar 4U 1907+09. *mnras* 421, 2079–2087. doi:10.1111/j.1365-2966.2012.20455.x, arXiv:1106.5957.
- Cusumano, G., di Salvo, T., Burderi, L., Orlandini, M., Piraino, S., Robba, N., Santangelo, A., 1998. Detection of a cyclotron line and its second harmonic in 4U1907+09. *aap* 338, L79–L82. doi:10.48550/arXiv.astro-ph/9809167, arXiv:astro-ph/9809167.
- Doroshenko, V., Santangelo, A., Ducci, L., Klochkov, D., 2012. Supergiant, fast, but not so transient 4U 1907+09. *aap* 548, A19. doi:10.1051/0004-6361/201220085, arXiv:1210.4428.
- Doroshenko, V., Santangelo, A., Suleimanov, V., 2011. Witnessing the magnetospheric boundary at work in Vela X-1. *aap* 529, A52. doi:10.1051/0004-6361/201116482, arXiv:1102.5254.
- Farinelli, R., Ceccobello, C., Romano, P., Titarchuk, L., 2012. Numerical solution of the radiative transfer equation: X-ray spectral formation from cylindrical accretion onto a magnetized neutron star. *aap* 538, A67. doi:10.1051/0004-6361/201118008, arXiv:1111.6851.
- Folkner, W.M., Williams, J.G., Boggs, D.H., Park, R.S., Kuchynka, P., 2014. The planetary and lunar ephemerides de430 and de431. Interplanetary network progress report 196, 42–196.
- Fritz, S., Kreykenbohm, I., Wilms, J., Staubert, R., Bayazit, F., Pottschmidt, K., Rodriguez, J., Santangelo, A., 2006. A torque reversal of 4U 1907+09. *aap* 458, 885–893. doi:10.1051/0004-6361:20065557, arXiv:astro-ph/0608518.
- Fürst, F., Suchy, S., Kreykenbohm, I., Barragán, L., Wilms, J., Pottschmidt, K., Caballero, I., Kretschmar, P., Ferrigno, C., Rothschild, R.E., 2011. Study of the many fluorescent lines and the absorption variability in GX 301-2 with XMM-Newton. *aap* 535, A9. doi:10.1051/0004-6361/201117665, arXiv:1110.2700.
- Giacconi, R., Kellogg, E., Gorenstein, P., Gursky, H., Tananbaum, H., 1971. An X-Ray Scan of the Galactic Plane from UHURU. *apjl* 165, L27. doi:10.1086/180711.
- Göğüş, E., Kreykenbohm, I., Belloni, T.M., 2011. Discovery of a peculiar dip from GX 301-2. *aap* 525, L6. doi:10.1051/0004-6361/201015905, arXiv:1011.3899.
- Harrison, F.A., Craig, W.W., Christensen, F.E., Hailey, C.J., Zhang, W.W., Boggs, S.E., Stern, D., Cook, W.R., Forster, K., Giommi, P., Grefenstette, B.W., Kim, Y., Kitaguchi, T., Koglin, J.E., Madson, K.K., Mao, P.H., Miyasaka, H., Mori, K., Perri, M., Pivovarov, M.J., Puccetti, S., Rana, V.R., Westergaard, N.J., Willis, J., Zoglauer, A., An, H., Bachetti, M., Barrière, N.M., Bellm, E.C., Bhalerao, V., Brejnholt, N.F., Fuerst, F., Liebe, C.C., Markwardt, C.B., Nynka, M., Vogel, J.K., Walton, D.J., Wik, D.R., Alexander, D.M., Cominsky, L.R., Hornschemeier, A.E., Hornstrup, A., Kaspi, V.M., Madejski, G.M., Matt, G., Molendi, S., Smith, D.M., Tomsick, J.A., Ajello, M., Ballantyne, D.R., Baloković, M., Barret, D., Bauer, F.E., Blandford, R.D., Brandt, W.N., Brenneman, L.W., Chiang, J., Chakrabarty, D., Chenevez, J., Comastri, A., Dufour, F., Elvis, M., Fabian, A.C., Farrah, D., Fryer, C.L., Gotthelf, E.V., Grindlay, J.E., Helfand, D.J., Krivonos, R., Meier, D.L., Miller, J.M., Natalucci, L., Ogle, P., Ofek, E.O., Ptak, A., Reynolds, S.P., Rigby, J.R., Tagliaferri, G., Thorsett, S.E., Treister, E., Urry, C.M., 2013. The Nuclear Spectroscopic Telescope Array (NuSTAR) High-energy X-Ray Mission. *apj* 770, 103. doi:10.1088/0004-637X/770/2/103, arXiv:1301.7307.
- in 't Zand, J.J.M., Baykal, A., Strohmayer, T.E., 1998. Recent X-Ray Measurements of the Accretion-powered Pulsar 4U 1907+09. *apj* 496, 386–394. doi:10.1086/305362, arXiv:astro-ph/9711292.
- in 't Zand, J.J.M., Strohmayer, T.E., Baykal, A., 1997. Dipping Activity in the X-Ray Pulsar 4U 1907+09. *apjl* 479, L47–L50. doi:10.1086/310570.
- Inam, S.Ç., Şahiner, Ş., Baykal, A., 2009. Recent torque reversal of 4U1907+09. *mnras* 395, 1015–1020. doi:10.1111/j.1365-2966.2009.14596.x, arXiv:0812.4189.
- Kreykenbohm, I., Wilms, J., Kretschmar, P., Torrejón, J.M., Pottschmidt, K., Hanke, M., Santangelo, A., Ferrigno, C., Staubert, R., 2008. High variability in Vela X-1: giant flares and off states. *aap* 492, 511–525. doi:10.1051/0004-6361:200809956, arXiv:0810.2981.
- Langer, S.H., Rappaport, S., 1982. Low-luminosity accretion onto magnetized neutron stars. *apj* 257, 733–751. doi:10.1086/160028.
- Leahy, D.A., 1991. Modelling observed X-ray pulsar profiles. *mnras* 251, 203. doi:10.1093/mnr/251.2.203.
- Leahy, D.A., Darbro, W., Elsner, R.F., Weisskopf, M.C., Sutherland, P.G., Kahn, S., Grindlay, J.E., 1983. On searches for pulsed emission with application to four globular cluster X-ray sources: NGC 1851, 6441, 6624 and 6712. *apj* 266, 160–170. doi:10.1086/160766.
- Maitra, C., Paul, B., 2013. Pulse-phase-dependent Variations of the Cyclotron Absorption Features of the Accreting Pulsars A0535+26, XTE J1946+274, and 4U 1907+09 with Suzaku. *apj* 771, 96. doi:10.1088/0004-637X/771/2/96,

- arXiv:1304.6252.
- Makishima, K., Kawai, N., Koyama, K., Shibasaki, N., Nagase, F., Nakagawa, M., 1984. Discovery of a 437.5-s X-ray pulsation from 4U 1907+09. *pasj* 36, 679–689.
- Marshall, N., Ricketts, M.J., 1980. Determination of a binary period for the variable X-ray source A 1907+09. *mnras* 193, 7P–13. doi:10.1093/mnras/193.1.7P.
- Mihara, T., 1995. Observational study of X-ray spectra of binary pulsars with Ginga. Ph.D. thesis. -.
- Miller, G.S., 1996. The Accretion Curtain and Pulse Phase Variations of the Bursting X-Ray Pulsar GRO J1744-28. *apjl* 468, L29. doi:10.1086/310231.
- Mukerjee, K., Agrawal, P.C., Paul, B., Rao, A.R., Yadav, J.S., Seetha, S., Kasturirangan, K., 2001. Pulse Characteristics of the X-Ray Pulsar 4U 1907+09. *apj* 548, 368–376. doi:10.1086/318655.
- Nespoli, E., Fabregat, J., Mennickent, R.E., 2008. Unveiling the nature of six HMXBs through IR spectroscopy. *aap* 486, 911–917. doi:10.1051/0004-6361/200809645, arXiv:0806.0295.
- Parmar, A.N., White, N.E., Stella, L., 1989. The Transient 42 Second X-Ray Pulsar EXO 2030+375. II. The Luminosity Dependence of the Pulse Profile. *apj* 338, 373. doi:10.1086/167205.
- Pradhan, P., Bozzo, E., Paul, B., 2018. Supergiant fast X-ray transients versus classical supergiant high mass X-ray binaries: Does the difference lie in the companion wind? *aap* 610, A50. doi:10.1051/0004-6361/201731487, arXiv:1711.10510.
- Riffert, H., Nollert, H.P., Kraus, U., Ruder, H., 1993. Fitting Pulse Profiles of X-Ray Pulsars: The Effects of Relativistic Light Deflection. *apj* 406, 185. doi:10.1086/172429.
- Roberts, M.S.E., Michelson, P.F., Leahy, D.A., Hall, T.A., Finley, J.P., Cominsky, L.R., Srinivasan, R., 2001. Phase-dependent Spectral Variability in 4U 1907+09. *apj* 555, 967–977. doi:10.1086/321487.
- Schwartz, D.A., Griffiths, R.E., Thorstensen, J.R., Charles, P.A., Bowyer, S., 1980. Optical identification of 4U 1907+09 using the HEAO-1 Scanning modulation collimator position. *aj* 85, 549–554. doi:10.1086/112710.
- Shakura, N., Postnov, K., Kochetkova, A., Hjalmarsdotter, L., 2012. Theory of quasi-spherical accretion in X-ray pulsars. *mnras* 420, 216–236. doi:10.1111/j.1365-2966.2011.20026.x, arXiv:1110.3701.
- Titarchuk, L., 1994. Generalized Comptonization Models and Application to the Recent High-Energy Observations. *apj* 434, 570. doi:10.1086/174760.
- Tobrej, M., Rai, B., Ghising, M., Tamang, R., Paul, B.C., 2023. A high-mass X-ray binary pulsar 4U 1907+09 with multiple absorption-line features in the spectrum. *mnras* 518, 4861–4869. doi:10.1093/mnras/stac3203, arXiv:2211.06038.
- Varun, Pradhan, P., Maitra, C., Raichur, H., Paul, B., 2019. Pulse Phase Variation of the Cyclotron Line in HMXB 4U 1907+09 with AstroSat LAXPC. *apj* 880, 61. doi:10.3847/1538-4357/ab2763, arXiv:1906.02917.
- Wang, Y.M., Welter, G.L., 1981. An analysis of the pulse profiles of the binary X-ray pulsars. *aap* 102, 97–108.